Citation
Akabar, N. and Chaturvedi, V. and Shillito, G.E. and Schwehr, B.J. and Gordon, K.C. and Huff, G.S. and Sutton, J.J. et al. 2019. Photophysical and biological investigation of phenol substituted rhenium tetrazolato complexes. Dalton Transactions. 48 (41): pp. 15613-15624. http://doi.org/10.1039/c9dt02198a

ARTICLE

Photophysical and Biological Investigation of Phenol and Methoxy Substituted Rhenium Tetrazolato Complexes

Received 00th January 20xx,
Accepted 00th January 20xx

DOI: 10.1039/x0xx00000x

www.rsc.org/

Nurshadrina Akabar,[a] Vishal Chaturvedi,[b] Georgina E. Shillito,[c] Bradley J. Schwehr,[a] Keith C. Gordon,[c] Gregory S. Huff,[c] Joshua J. Sutton,[c] Brian W. Skelton,[d] Alexandre N. Sobolev,[d] Stefano Stagni,[e] Delia J. Nelson,[b] and Massimiliano Massi[a,*]

The synthesis, structural and photophysical characterisation of four tricarbonyl rhenium(I) complexes bound to 1,10-phenanthroline and a tetrazolate ancillary ligand are reported. The complexes are differentiated by the nature (hydroxy or methoxy) and position (*meta* or *para*) of the substituent attached the phenyl ring in conjugation to the tetrazole ring. The complexes exhibit phosphorescent emission from triplet charge transfer excited states, with maxima around 600 nm, excited state lifetime decays in the 200-300 ns range, and quantum yield values of 4-6% in degassed acetonitrile solutions. The nature and position of the substituent does not significantly affect the photophysical properties, which remain unchanged even after deprotonation of the hydroxide group on the phenol ring. The interpretation of the photophysical data was further validated by resonance Raman spectroscopy and time-dependent density functional theory calculations. All the complexes are internalised within cells, albeit with variable degree. As highlighted by a combination of flow cytometry and confocal microscopy, the species display diffuse cytoplasmic localisation aside for the complex with the hydroxy functional group in the *para* position, which reveals lower accumulation in cells and more pronounced punctate staining. Overall, the complexes displayed low levels of cytotoxicity.

Introduction

The photophysical properties of phosphorescent metal complexes (e.g. Re^{+}, Ru^{2+}, Ir^{3+}, Pt^{2+}, and Au^{+}) have been at the centre of intensive scientific investigation, not only from a fundamental point of view, but also for their favourable application in many areas of science and technology. One of the major fields where phosphorescent transition metal complexes have been - and continues to be - explored is life sciences.[1-3] In fact, these compounds possess a combination of properties such as large Stokes shifts, long luminescent lifetimes, visible light excitation and emission and distinct resistance to photobleaching, that make them suitable candidates for biological applications[4-6] including optical imaging, cellular labelling and sensing.[7-18] These properties are favourable as they have the potential to overcome drawbacks that are commonly associated with traditional organic fluorophores. Transition metal complexes also have the capacity to sensitise singlet oxygen,[19] $^1O_2$, depending on the imaging technique and conditions. While this is a commonly unwanted process in cellular imaging, due to the cytotoxicity of this reactive species, it represents a useful property in the design of theranostic agents, especially when the ability to sensitise $^1O_2$ can be controlled within cellular environments.[20]

Most of the studies involving phosphorescent rhenium complexes have been centred around the archetypal structure *fac*-[Re(diim)$(CO)_3$L], where diim represents a bidentate diimine ligand and L is a monodentate ancillary ligand. The photophysical and physico-chemical properties of these complexes can be easily tuned by chemical variation of diim and L to optimise the compounds for use in life sciences.[21] In particular, the phosphorescence properties of these complexes can be generally ascribed to excitation to metal-to-ligand charge transfer (MLCT) states, with potential admixtures of ligand-to-ligand charge transfer (LLCT) states depending on the chemical nature of the ligand L. These admixed states are often referred to as metal-ligand-to-ligand charge transfer (MLLCT).

During our studies, we have investigated the use of *fac*-[Re(diim)$(CO)_3$L] complexes, where L is a variably substituted 5-aryl tetrazolato ligand, in biological imaging.[22] The results obtained to date indicate that these complexes are viable building blocks for the design of cellular markers for optical imaging. We were able to determine that variations in the functional groups of the ancillary ligand has a profound influence on the biological properties of the complexes. In particular, efficient staining of lipid droplets and endoplasmic

[a] School of Molecular and Life Sciences, Curtin Institute for Functional Materials and Interfaces, Curtin University, Bentley WA, Australia. Email: m.massi@curtin.edu.au
[b] School of Biomedical Sciences, Curtin Health Innovation Research Institute, Curtin University, Bentley WA, Australia.
[c] Department of Chemistry Te Tari HuaRuanuk, University of Otago, Dunedin, New Zealand.
[d] School of Molecular Sciences and CMCA, The University of Western Australia, Perth WA, Australia.
[e] Department of Industrial Chemistry Toso Montanari, University of Bologna, Bologna, Italy.
Electronic Supplementary Information (ESI) available: NMR spectra, selected bond lengths and angles for crystal structures, TDDFT calculations, and Raman spectra. See DOI: 10.1039/x0xx00000x

reticulum was achieved,[23-25] with the probes being mostly non-toxic and resistant to photobleaching, thus allowing imaging for longer timescales.

Continuing our work in this area, we wanted to explore rhenium tetrazolato complexes whose luminescence properties might be somewhat dependent on the pH of the cellular environment. For this scope, we designed and synthesised rhenium complexes where the tetrazole ring of the ancillary ligand is conjugated to a phenol substituent (Figure 1). Furthermore, the corresponding complexes with a methoxy substituent were prepared to carefully assess photophysical changes in complexes that could be deprotonated compared to complexes without acidic protons. Phenol groups incorporated within luminescent metal complexes are capable of introducing photoinduced electron transfer (PeT) processes.[1, 2, 26-28] What makes phenols attractive to study electron transfer is the fact that phenols can act as both electron and proton donors.[29] In most PeT-based probes, deprotonation of the phenol can promote PeT, resulting in emission quenching. There have been quite a few examples of pH-dependent complexes carrying phenolic PeT groups based on organic dyes.[26, 30, 31] Only recently, increasing interest has been shifted towards electron transfer of photoexcited molecules or metal complexes.[29, 32, 33 34, 35]

The work presented herein describes the synthesis and photophysical properties of the complexes shown in Figure 1. Contrary to previous example of pH-sensitive complexes, these compounds do not exhibit PeT processes even upon deprotonation of the phenol moieties. The experimental findings were supported with the use of Raman spectroscopy and time-dependent density functional theory (TDDFT). The complexes are further assessed as cellular markers in optical imaging by confocal microscopy. Furthermore, their use in flow cytometry is explored, revealing these complexes are useful markers for this technique, possessing conveniently distanced excitation and emission profiles.

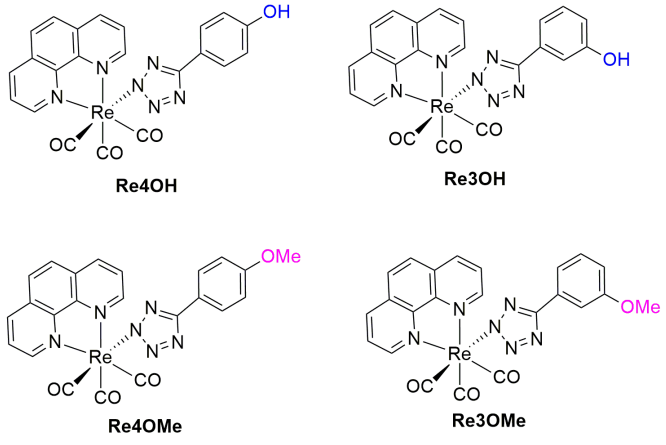

Figure 1. Structures of rhenium(I) tetrazolato complexes prepared in this work.

Results and Discussion

Synthesis and structural characterisation of the rhenium(I) tetrazolato complexes

The tetrazole ligands were synthesised following the methodology reported by Koguro, which involves a 1,3-dipolar cycloaddition of sodium azide onto the corresponding nitrile-containing substrates in toluene (see Scheme 1).[36] The formation of the targeted ligands were confirmed by the presence of the typical N-H and C=N stretching peaks around 3100 and 1600 cm^{-1} in the IR spectra, respectively.

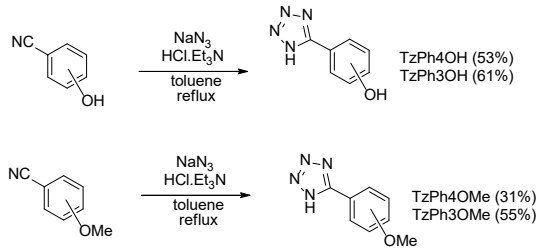

Scheme 1. Reaction schemes adopted for the preparation of the tetrazole-functionalised ligands.

To prepare the neutral rhenium(I) complexes **Re4OMe** and **Re3OMe**, the halogenated *fac*-[Re(phen)$(CO)_3$Cl] precursor was reacted with the corresponding ligand and triethylamine in an ethanol/water mixture at reflux overnight (Scheme 2). The pure complex **Re4OMe** could be filtered from the reaction mixture, whereas **Re3OMe** was purified by flash column chromatography on an alumina stationary phase. On the other hand, the complexes **Re4OH** and **Re3OH** were prepared by reaction of *fac*-[Re(phen)$(CO)_3$Cl] with the corresponding ligand and triethylamine in an acetonitrile/methanol mixture under microwave irradiation for a couple of hours and temperature range of 130-160 °C (Scheme 2), leading to the pure complexes that were purified by simple filtration from the reaction mixture. The proposed structures were supported by the typical intense peaks in 2020-1800 cm^{-1} region of the IR spectra, by ^1H and ^{13}C NMR spectroscopy (see SI for the corresponding NMR spectra), elemental analysis and X-ray diffraction.

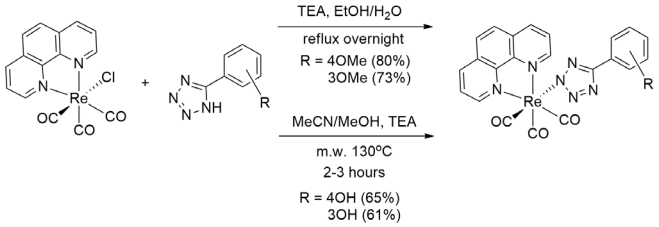

Scheme 2. Reaction scheme for the preparation of the target rhenium(I) complexes.

Single crystals suitable for X-ray diffraction were grown for all the complexes (Figure 2). Table containing data on bond lengths and angles can be found in the SI. In all cases, the rhenium centre is bound to the N2 atom of the tetrazole ring, consistently with previously reported analogous complexes.[37, 38] The coordination geometry appears as a slightly distorted octahedron, with the three CO ligands arranged in a *facial*

configuration, as preliminarily suggested by the analysis of the corresponding IR spectra. The tetrazole and phenyl rings are approximately co-planar to maximise interannular conjugation.

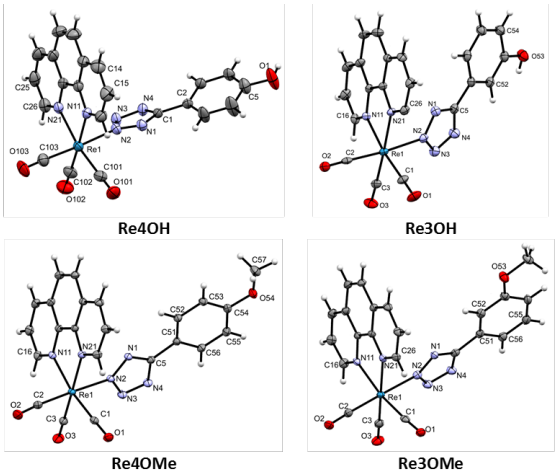

Figure 2. Crystal structure of the synthesised rhenium(I) complexes with displacement ellipsoids drawn at 50% probability.

The complex **Re3OH** forms hydrogen-bonded pairs in its structure, as shown in Figure 3. Specifically, the N3 atom of the tetrazole ring is bound to the OH group of the paired complex, and the two complexes are related by a pseudo inversion centre.

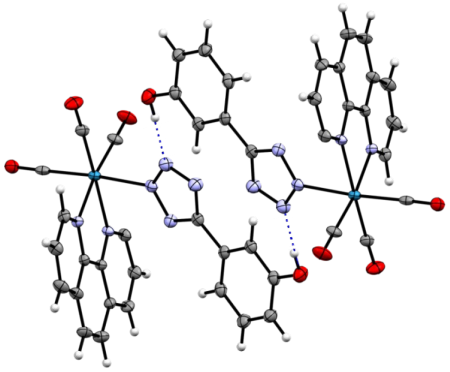

Figure 3. Crystal structure of **Re3OH** highlighting the formation of hydrogen bonded pairs. Hydrogen bonds are highlighted with dashed lines.

Table 1. Photophysical data for the synthesised rhenium(I) complexes measured from diluted acetonitrile solutions (10^{-5} M).

	298 K						77 K	
	λ_{abs} [nm] ($10^4\varepsilon$ [$M^{-1}cm^{-1}$])	λ_{em} [nm]	τ [ns][a]	τ [ns][b]	Φ[a, c]	Φ[b, c]	λ_{em} [nm]	τ [µs]
Re4OH	259 (3.74), 365 (0.30)	600	86	202	0.012	0.064	545	8.50
Re3OH	257 (3.27), 367 (0.26)	604	87	206	0.010	0.042	551	5.29
Re4OMe	259 (4.20), 364 (0.35)	613	85	212	0.011	0.046	537	10.64 (67%), 3.88 (33%)
Re3OMe	257 (3.50), 369 (0.37)	608	100	299	0.010	0.036	540	8.46

[a] air equilibrated solution; [b] degassed solution; [c] quantum yield Φ measured against an air equilibrated solution of quinine sulfate in 1 M H_2SO_4.

Photophysical investigation

The photophysical properties of the complexes were studied in diluted acetonitrile solutions at room temperature and frozen matrix at 77 K, with the corresponding spectra shown in Figure 4 and 5. A summary of the photophysical data is provided in Table 1.

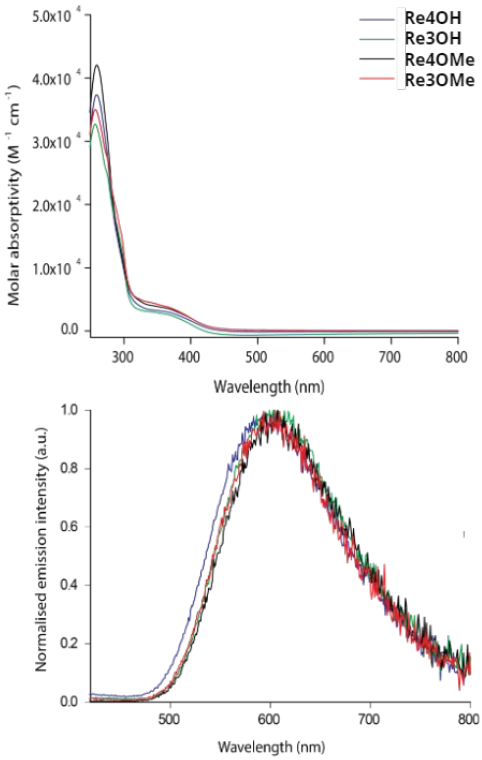

Figure 4. Absorption (top) and emission (bottom) spectra for Re(I) tetrazolato complexes from diluted acetonitrile solution (10^{-5} M). The emission spectra were recorded using an excitation wavelength of 360 nm.

In general, the absorption profiles (Figure 4, top) were found to be similar for all of the complexes, displaying an intense (ε ≈ 3.27x10⁴ - 4.20x10⁴ $M^{-1}cm^{-1}$) higher energy band in the 250-300 nm region, followed by a band of lower intensity (ε ≈ 0.26x10⁴ - 0.37x10⁴ $M^{-1}cm^{-1}$) in the 300-450 nm region. The higher energy band was attributed to intraligand (IL) transitions localised on the 1,10-phenanthroline (phen) and tetrazole ligands, while the lower energy band was attributed to metal-to-ligand charge transfer (MLCT) transitions mainly involving the 5d orbitals of the rhenium centre and the accessible π* orbitals of the phen ligand. These transitions are partially mixed with ligand-to-ligand charge transfer (LLCT) transitions involving the tetrazole ring and the phen ligand, as previously observed for similar types of rhenium(I) tetrazolato complexes.[37]

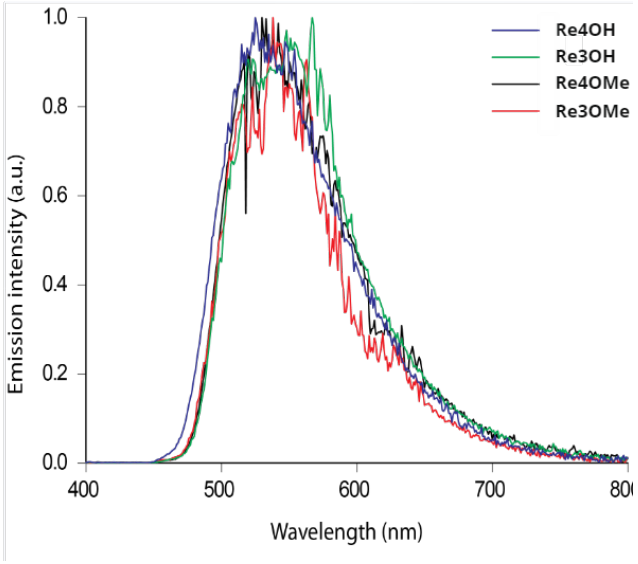

Figure 5. Emission profiles for substituted Re(I) tetrazolato complexes at 77 K. The emission spectra were recorded using an excitation wavelength of 360 nm.

To support the assignment of the transitions from the absorption spectra, TDDFT calculations were performed. The associated results predict that a number of weak transitions contribute to the 300-450 nm absorption band (see SI). These states involve a number of different molecular orbitals of mixed metal and ligand character and therefore suggest that the low energy absorption band is attributed to a MLLCT state. The HOMO is delocalised over both the metal and the tetrazole ligand, while the LUMO is largely phen based (Figure 6). The HOMO→LUMO transition is comparatively weak and may contribute to the red-tail of the lowest-energy absorption band. The higher energy states which likely contribute to the 250-300 nm band, still show some metal contribution but exhibit more ligand character. These results are in agreement with a previous study performed by Werrett *et al.*[37] The simulated electronic data showed minimal variation between the complexes, which is consistent with the small variation in both molar absorptivity and absorption maxima in the experimental UV-vis spectra.

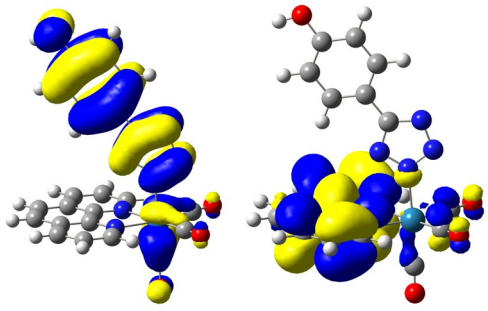

Figure 6. Localisation of the HOMO (left) and LUMO (right) as calculated from TDDFT for complex **Re4OH**.

DFT optimisation and frequency calculations show the presence of several local minima in the complexes, which are approximately isoenergetic. As noted by Werret *et al.*, these confirmations can be obtained through rotation of the tetrazole ligand orthogonal to the plane of the phen ligand (see SI). When

TDDFT calculations were performed on the various confirmations, slight differences in the predicted energies and oscillator strengths were observed. However, the nature of the molecular orbitals did not appear to be affected. Due to their near isoenergetic nature, averaged calculated TDDFT data from the different conformers are presented (see SI).[37]

Following excitation at 360 nm, each of the neutral tetrazolato rhenium(I) complexes exhibit a broad and structureless emission band in the 500-800 nm region at room temperature (Figure 4). The emission profiles appear virtually superimposable for the four complexes, supporting the similarity between the various emitting excited states. The broad and structureless nature of these bands is typical of charge transfer (CT) states.[39] The excited state lifetime decays (τ) of the complexes are also similar. In all cases, the decay data could be fitted with monoexponential functions. The values of τ are relatively long and in the range 200-300 ns in degassed acetonitrile solutions. These values are typical of neutral rhenium complexes with emission maxima around 600 nm. Therefore, the emitting state is described as ^{3}MLLCT. The triplet multiplicity is also supported by the sensitivity to the presence of oxygen. In fact, air equilibrated acetonitrile solutions display shorter values of τ (85-100 ns) and a decrease in quantum yield from 4-7% to about 1%. The similarity of the photophysical data for the four complexes with previously reported rhenium(I) tetrazolato complexes suggest that the nature of the substituent on the aromatic ring conjugated to the tetrazole does not significantly influence the relative energy of the emissive ^{3}MLLCT state.

The emission of the complexes was also measured in frozen acetonitrile matrix at 77 K (Figure 5). All the spectra appear consistently blue-shifted by about 50-60 nm. This behaviour is consistent with rigidochromism,[37, 40] as typical of emission from excited states of charge transfer nature. The excited state lifetime decay values elongate to a range of 5-11 µs.

Deprotonation studies of the phenol functionalised complexes

To investigate whether the phenol functionalised complexes might be susceptible to the quenching of ^{3}MLLCT state, deprotonation studies were attempted. The potential deprotonation of the phenol ring was monitored by means of ^{1}H NMR spectroscopy, in particular by monitoring changes to the chemical shift of the peaks belonging to the H atoms of the phenol ring.

Initially, the complexes **Re3OH** and **Re4OH** were treated with triethylamine in acetonitrile, up to an excess of 2.0 equivalents. However, no changes in the ^{1}H NMR spectra were detected by sequential addition of base. Therefore, potassium *tert*-butoxide (KO^{t}Bu) was chosen as a stronger base. The addition of 1.0 equivalent of KO^{t}Bu to a deuterated methanol solution containing either **Re3OH** or **Re4OH** caused detectable changes in the ^{1}H NMR spectra of the complexes as shown in Figure 7.

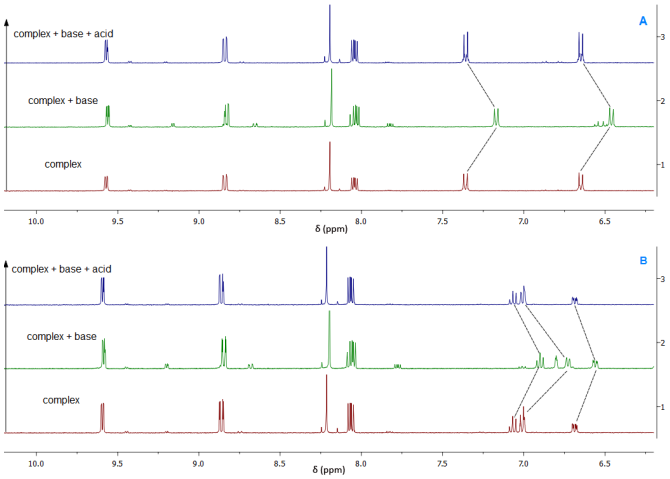

Figure 7. Comparison of ^{1}H NMR spectra obtained from deuterated methanol solutions containing complex **Re4OH** (A) and complex **Re3OH** (B). For each complex, the initial ^{1}H NMR spectrum is displayed (bottom), along with the addition of base (base), and the sequential addition of acid to reprotonate the phenol ring. The relative changes in the peaks corresponding to the H atoms of the phenol rings are highlighted by the dashed lines.

Upon addition of base, all the peaks belonging to the H atoms of the phenol ring resulted in shielding of variable degree. The upfield chemical shift is consistent with increased electron density on the phenolate ring caused by the deprotonation. No significant change is observed in the four peaks of the aromatic H atoms of the phen ligand. To support the fact that the changes to the ^{1}H NMR spectra were due to reversible deprotonation of the phenol ring, one equivalent of 10-camphosulphonic acid was added to the solution containing the rhenium complexes and KO^{t}Bu. As seen in Figure 7, upon addition of acid the peaks corresponding to the H atoms of the phenol ring return to the values of their initial chemical shifts.

To assess whether the presence of the phenolate anion would cause quenching of the ^{3}MLLCT excited state (e.g. photoinduced electron transfer), the excited state lifetime decay was recorded for the complexes in methanol before and after the addition of one equivalent of KO^{t}Bu, with the corresponding values reported in Table 2. From the data, and the fact that no significant decrease was detected in the emission intensity and maxima before and after the addition of the base, it can be concluded that the increased electron density of the phenolate anion does not induce quenching of the ^{3}MLLCT excited state of the rhenium. Furthermore, the lack of shift in the emission maxima indicates that the deprotonation of the ligand does not result in an indirect increased electron density on the rhenium centre through the tetrazole ring, as this effect would be expected to result in a red-shift of the emission maxima due to a destabilisation of 5d orbitals.

TDDFT calculations were performed on the optimized structures of the deprotonated phenol complexes. A number of additional transitions with negligible oscillator strengths were predicted, however, the lowest energy transitions with appreciable intensity ($f > 0.01$) were largely of MLLCT character and were predicted to occur at similar energies to the protonated species (Table S8).

Table 2. Excited state lifetime decay values for the rhenium(I) complexes measured from air-equilibrated diluted methanol solutions (10^{-5} M).

	τ [ns] initial conditions	τ [ns] + 1 eq. KO^{t}Bu
Re4OH	93	94
Re3OH	131	128
Re4OMe	119	119
Re3OMe	132	131

Resonance Raman studies

Resonance Raman spectra of the complexes in methanol were obtained with 355 nm excitation. As the excitation wavelength is coincident with the low energy absorption band, selective vibrational modes show enhancement, relative to the non-resonance spectrum. The specific nature of these vibrations can be utilised to aid in characterisation of the excited state in resonance.[41-43] Solvent subtraction and subsequent baseline correction were applied to the resonance spectra, due to the limited solubility of the complexes. A certain degree of care must be therefore taken in comparing the resonant spectrum and non-resonant spectrum, which was taken at 1064 nm on a solid sample. Nevertheless, some spectral differences are clearly distinguishable. As shown in Figure 8, the totally symmetric CO stretching mode at 2031 cm^{-1} of **Re4OH** is significantly enhanced compared to the non-resonant spectrum, indicating clear involvement of the rhenium centre in the resonant excited state. Modes at 1585 and 1520 cm^{-1}, which are attributed to vibrations of the phen ligand, show an increase in intensity, alongside bands at 1632, 1147 and 1258 cm^{-1}, which likely have some contribution from the tetrazole ligand. These data are consistent with the TDDFT assignment of the MLLCT state in this region.

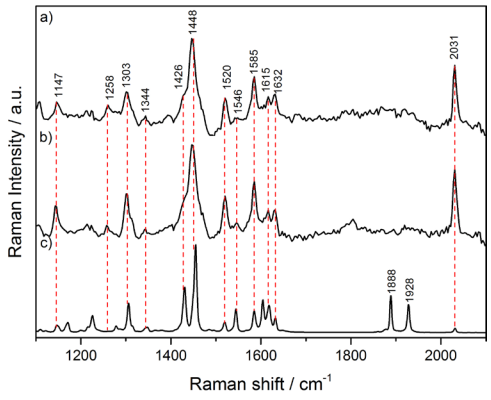

Figure 8. Raman spectra of **Re4OH**. 351 nm resonance spectra are shown in methanol (a) and methanol with 1 equivalent of KO^{t}Bu (b). Panel c) shows the non-resonant 1064 nm spectrum from a solid state sample.

The non-resonant spectra showed minimal variation between complexes due to their structural similarity (see SI). Likewise, the resonance spectra displayed similar enhancement patterns, reinforcing the hypothesis that the populated excited state is not affected by the position or nature of the phenyl ring substituent. The solubility of the complexes was somewhat improved upon addition of an equivalent of KO^{t}Bu, but as illustrated in Figure 8, no notable spectral changes were observed.

Biological investigation

To evaluate the compatibility of the complexes and their potential use as cellular markers, it is important to assess their lipophilic character. The *n*-octanol/water distribution coefficients (log$D_{7.4}$) of the complexes were measured using the shake-flask method[44, 45] and the obtained values are summarised in Table 3. The value of log$D_{7.4}$ is similar for the complexes and within the expected range for neutral rhenium(I) tetrazolato complexes.[44] The only notable difference is the relative value of log$D_{7.4}$ of **Re3OH**, which is larger than the values of all the other three complexes. Interestingly, the X-ray crystal structure of the complex showed the formation of hydrogen bonded pairs in the solid state, and it might be possible that its partial or complete retention in solution could be the reason why this complex is slightly more lipophilic in comparison to the others.

Table 3. Distribution coefficient (log$D_{7.4}$) values for the complexes obtained from *n*-octanol/water solutions.

	log$D_{7.4}$
Re4OH	1.55 ± 0.03
Re3OH	2.10 ± 0.08
Re4OMe	1.49 ± 0.05
Re3OMe	1.25 ± 0.05

The cellular internalisation of the four complexes was initially investigated by means of flow cytometry. JU77 tumour cells were incubated with the complexes for 30 minutes before the analysis. Figure 9 shows representative plots of gated viable cells (stained with Zombie NIR™ Fixable Viability Kit) upon incubation at varying concentrations of 5, 10 and 20 µM. Consistent with the photophysical data, the emission of the complexes was obtained in the 605±12 nm channel upon UV excitation at 350 nm.

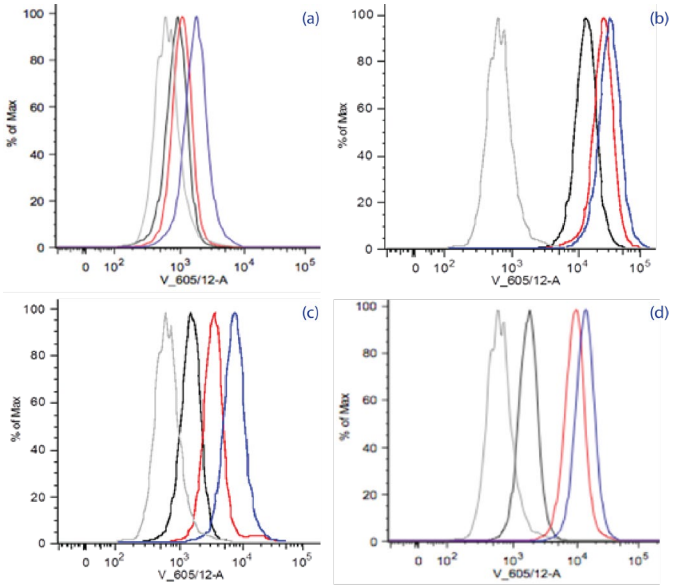

Figure 9. Representative flow cytometry histogram data of mean fluorescence intensities for JU77 cells stained with complexes **Re4OH** (a), **Re3OH** (b), **Re4OMe** (c), and **Re3OMe** (d) **5-8** at concentrations of 5 μM (black), 10 μM (red), 20 μM (blue) compared to unstained control cells (grey trace). All cells were stained with Zombie NIR to detect gate viable cells. The data are representative from reproducible experiments performed three times. The emission signal was detected in the 605±12 nm channel (V_605/12-A) upon excitation at 350 nm.

The flow cytometry data suggest differences in the cellular incubation of the complexes. Notably, the *meta* substituted complex **Re3OH** seems to be the most efficient in being internalised within the cells, and this result might be correlated with the highest value of log$D_{7.4}$ out of the complexes. On the other hand, the complex **Re4OH** does not seem to be efficiently incubated even at the highest concentration of 20 μM. In this case, only a low cell number of stained viable cells were detected (1071 cells), a value that was slightly above the control cells. The complexes **Re4OMe** and **Re3OMe** follow an analogous trend. **Re4OMe** demonstrates a clear dose-related staining response with a medium count of 3457 emissive cells. Its *meta* derivative **Re3OMe** also shows a clear dose-related staining response with the two highest concentrations delivering very bright signals in association with a higher count of 10492 stained cells.

The complexes were also investigated via spinning disk confocal microscopy using excitation at 405 nm, upon incubation of RAW264.7 cells for 30 minutes at a concentration of 10 μM. The cells were then fixed prior to imaging using 4% paraformaldehyde in PBS. The confocal images for the cells incubated with the rhenium complexes are reported in Figure 10. Examination of individual cells showed a generalised and cytoplasmic staining for all rhenium complexes except complex for **Re4OH**. In all cases, no nuclear staining was observed. Complex **Re4OH** shows a very punctate pattern inside the cells with diffused signal throughout the cytoplasm. The overall signals from cells stained with **Re4OH** seems lower compared to cells stained with the other three complexes, an observation that is in agreement with the results obtained via flow cytometry.

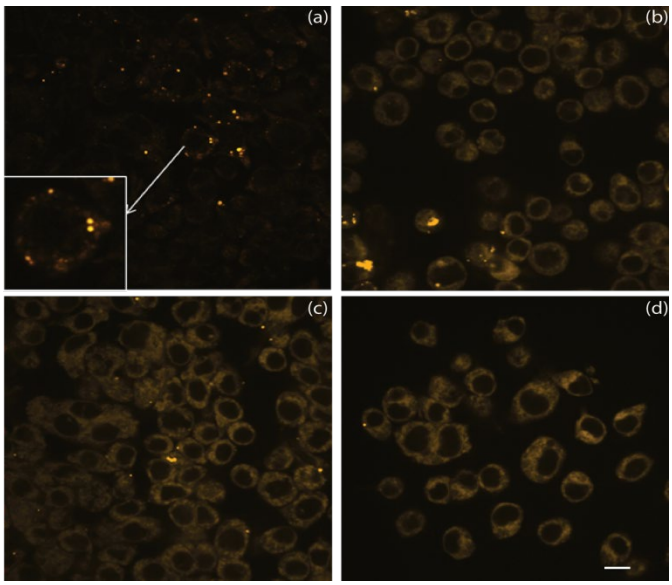

Figure 10. Confocal imaging of RAW264.7 cells incubated with the rhenium complexes for 30 minutes at 10 μM concentration: **Re4OH** (a), **Re3OH** (b), **Re4OMe** (c), and **Re3OMe** (d) The cells are then fixed using using 4% paraformaldehyde in PBS. Scale bar = 100 μm.

The cytotoxicity of the rhenium complexes was assessed in both JU77 and RAW264.7 cells. The extent of cell death was analysed by comparing stained and control unstained cells. The ratio of live and dead cells in each case was assessed using a Zombie NIR™ dye, detected by flow cytometry, which is only permeabilised in dead cells due to a compromised cellular membrane. The cytotoxicity was assessed after incubation of the cells with the rhenium complexes at concentration values of 5, 10, and 20 μM for a period of 30 minutes. The obtained results are shown in Figure 11. All JU77 and RAW264.7 cell populations were significantly different ($p < 0.05$) to the control. As it can be seen from the data, none of the rhenium complexes exhibited acute cytotoxicity, even at the highest concentration of 20 μM. The percentage of cell death never exceeded 15%, with cell death measured in the control unstained sample measured at 6%. The low cytotoxicity is consistent with previously published results on rhenium tetrazolato complexes,[44, 46] which are not prone to ligand exchange. It is in fact well known that ligand substitution reactions occurring within cells are responsible to the cytotoxicity of rhenium complexes.

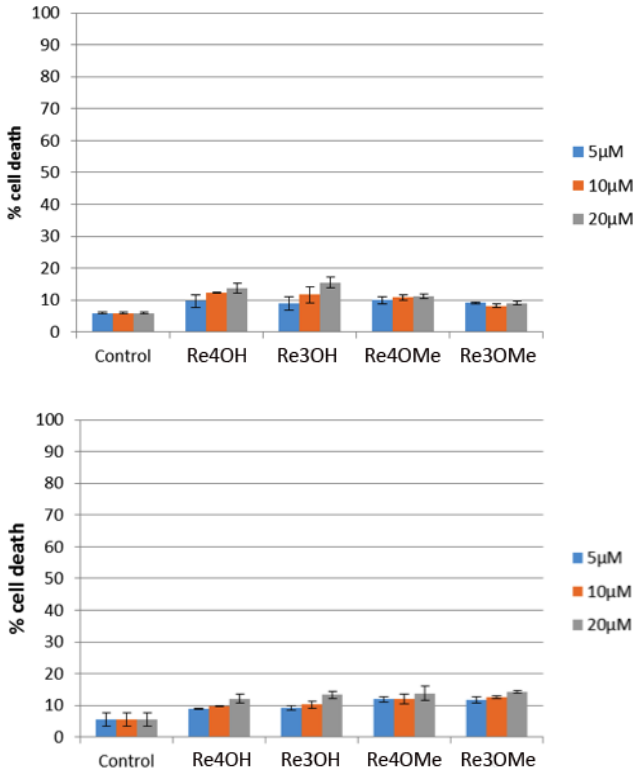

Figure 11. Live/dead assay of on JU77 (top) RAW264.7 cells (bottom) stained with the rhenium complexes as compared to control unstained cells. Error bars indicate the standard deviation of three independent measurements.

Conclusions

Four neutral rhenium(I) tetrazolato complexes of general formulation *fac*-[Re(phen)$(CO)_3$L] have been synthesised and characterised, with chemical variations on the tetrazolato ligands L. Specifically, the tetrazolato ring is conjugated to a phenol or a methoxybenzene ring with the substituent either in the *para* or *meta* position. The complexes could be efficiently prepared by direct exchange of the halide ligand in *fac*-[Re(phen)$(CO)_3$Cl] with the appropriate tetrazole anion using microwave irradiation for a couple of hours. The structure of all the four complexes could be confirmed via single crystal X-ray diffraction. The photophysical investigation has revealed phosphorescent emission from ^{3}MLLCT excited states, with values of quantum yield and excited state lifetime decay typical for neutral rhenium(I) tetrazolato complexes. No photoinduced electron transfer processes could be detected for these complexes, as the photophysical properties did not change even after deprotonation of the phenol rings. The results indicate that variations of the electronic density on the conjugated species bound to the tetrazolato ring have small influence on the ground or excited states on the rhenium centre. These conclusions were also supported by means of resonance Raman spectroscopy and TDDFT calculations. The complexes were also assessed as cellular markers in tumour JU77 and RAW264.7 cells by means of flow cytometry and confocal microscopy. The complexes internalised well within the cells, aside for the complex functionalised with the 4-phenol group, which showed lower accumulation and more punctate staining. The remaining complexes displayed diffused cytoplasmic localisation and absence of nuclear staining. The toxicity was also evaluated, revealing lack of acute cytotoxicity with incubation concentrations up to 20 µM, for 30 minutes. The low toxicity might be ascribed to the absence of ligand exchange reactions occurring within the cells.

Conflicts of interest

Rhenium complexes of similar structure are commercialised by ReZolve Scientific as cellular markers for lipid imaging. MM is a shareholder of ReZolve Scientific.

Experimental procedure

General considerations

All reagents and solvents were purchased from Strem Chemicals, Sigma Aldrich, Alfa Aesar or AK Scientific and used as received without further purification. Melting points were determined using the BI Barnsted Electrothermal 9100 melting point apparatus and are reported uncorrected. Infrared spectra were obtained on a Perkin-Elmer Spectrometer 100 FTIR using an attenuated total reflectance attachment with a diamond stage. The spectra were recorded with samples in the solid state and were scanned from 4000 to 650 cm^{-1}. The intensities of the IR bands are reported as strong (s), medium (m), or weak (w), with broad (br) and shoulder (sh) bands also specified. Nuclear magnetic resonance (NMR) spectra were recorded on an Ultrashield Bruker Avance 400 spectrometer, where all ^{1}H NMR spectra were obtained at a 400 MHz frequency and all ^{13}C NMR spectra were obtained at a 100 MHz frequency at room temperature. ^{1}H and ^{13}C chemical shifts were referenced to residual solvent signals. Elemental analyses were obtained at the Central Science Laboratory, University of Tasmania (Australia) using a Thermo Finnigan EA 1112 Series Flash, or at the School of Molecular and Life Sciences, Curtin University, using a Perkin Elmer EA 2400.

Synthesis of the ligands

The synthesis of the functionalised 1H-5-aryltetrazoles was adapted from a previously published procedure by Koguro *et al.*[36] In general, triethylamine (1.2 eq) and hydrochloric acid (32%, 1.2 eq) were combined in toluene (*ca.* 10 mL) at 0 °C within a stoppered round bottom flask, and vigorously stirred for 10 min. The corresponding nitrile (1.0 eq; 4-methoxybenzonitrile, 3-methoxybenzonitrile, 4-hydroxybenzonitrile, 3-hydroxybenzonitrile) and sodium azide (1.2 eq) were added and the mixture was heated at reflux overnight. After cooling to room temperature, water (*ca.* 5 mL) was added. The aqueous phase was extracted, followed by dropwise addition of hydrochloric acid (1 M). The resulting precipitate was collected by vacuum filtration, washed with cold water and air-dried to afford the corresponding targeted compound.

1H-(4-hydroxyphenyl)tetrazole. Yield: 448 mg (60%). ν_{max}(ATR-FTIR)/cm^{-1}: 3412 s (br, OH), 2708-2622 s (br), 1646 w, 1613 s, 1599 s, 1514 m, 1468 m, 1414 s, 1279 m, 1181 m, 1079 m, 835 w, 519 w. ^{1}H NMR (δ, ppm, DMSO-d_6): 10.18 (1H, s), 7.87 (2H, d, *J* = 8.9 Hz), 6.96 (2H, d, *J* = 8.9 Hz).

1H-(3-hydroxyphenyl)tetrazole. Yield: 457 mg (61%). ν_{max}(ATR-FTIR)/cm^{-1}: 3461 s (br, OH), 2629 s (br), 1656 m, 1623 w, 1588 s, 1573 s, 1487 s, 1410 m, 1253 m, 1236 s, 1024 m, 744 w, 682 w. ^{1}H NMR (δ, ppm, DMSO-d_6): 9.94 (1H, s), 7.52-7.42 (2H, m), 7.38 (1H, app. t, *splitting* = 8.1), 6.98-6.95 (1H, m).

1H-(4-methoxyphenyl)tetrazole. Yield: 117 mg (31%). ν_{max}(ATR-FTIR)/cm^{-1}: 3100-2500 s (br), 1614 w, 1499 m, 1441 m, 1407 m, 1328 m, 1299 m, 1263 s, 1183 m, 1034 m, 834 w, 749 w, 612 w. ^{1}H NMR (δ, ppm, $CDCl_3$): 7.98 (2H, d, *J* = 8.0 Hz), 7.16 (2H, d, *J* = 8.0 Hz), 3.84 (3H, s).

1H-(3-methoxyphenyl)tetrazole. Yield: 226 mg (55%). ν_{max}(ATR-FTIR)/cm^{-1}: 3096-2621 s (br), 1655 m, 1619 w, 1585 s, 1563 s, 1490 s, 1439 m, 1287 m, 1398 w, 1287 m, 1234 s, 1141 m, 1046 m, 1001 m, 797 m, 745 m, 683 w. ^{1}H NMR (δ, ppm, DMSO-d_6): 7.69-7.58 (2H, m), 7.52 (1H, app. t, *splitting* = 8.4 Hz), 7.17 (1H, d, *J* = 8.4 Hz), 3.84 (3H, s).

Synthesis of complexes Re4OH and Re3OH

The starting precursor *fac*-[Re(phen)(CO)$_3$Cl] and 1.4 equivalents of the corresponding ligand were combined with 1.4 equivalents of triethylamine in a 4:1 mixture of acetonitrile and methanol, in a microwave vial. This mixture was heated in a Biotage microwave reactor for 2 hours, with maximum temperature set in the range 130-160 °C.

Re4OH. Light yellow star-like needles precipitated over time (the formation of the precipitate was induced by scratching the flask with a metallic spatula), were collected via vacuum filtration, and washed with acetonitrile. Yield: 45 mg (65%). ν_{max} (ATR-FTIR)/cm^{-1}: 3070 m (OH), 2024 s (CO), 1931 m (CO), 1893 s (CO). ^{1}H NMR (δ, ppm, DMSO-d_6): 9.56 (2H, d, *J* = 8.0 Hz), 9.51 (1H, s), 8.98 (2H, d, *J* = 8.3 Hz), 8.31 (2H, s), 8.12 (2H, d, *J* = 8.3 Hz), 7.31 (2H, d, *J* = 8.7 Hz), 6.64 (2H, d, *J* = 8.7 Hz). ^{13}C NMR (δ, ppm, DMSO-d_6): 197.0 (CO), 194.2 (CO), 162.3 (CN_4), 157.7, 154.2, 146.5, 139.7, 130.3, 127.7, 126.9, 126.7, 120.3, 115.3. Elemental Analysis: Calc for $C_{22}H_{13}N_6O_4Re{\cdot}0.2H_2O$: C (42.95%), H (2.20%), N (13.66%); found C (42.51%), H (1.67%), N (13.56%). Single crystals suitable for X-ray diffraction were grown by slow diffusion of diethyl ether into a dichloromethane solution of the complex.

Re3OH. A Light yellow precipitate formed over time (the formation of the precipitate was induced by scratching the flask with a metallic spatula), was collected via vacuum filtration, and washed with acetonitrile. Yield: 45 mg (61%). ν_{max} (ATR-FTIR)/cm^{-1}: 3072 m (OH), 2021 s (CO), 1896 s (br, CO). ^{1}H NMR (δ, ppm, DMSO-d_6): 9.56 (2H, d, *J* = 6.4 Hz), 9.40 (1H, s br), 8.99 (2H, d, *J* = 8.3 Hz), 8.31 (2H, s), 8.13 (2H, d, *J* = 8.3 Hz), 7.05 (1H, app. t, *splitting* = 7.9 Hz), 6.99 (s, 1H), 6.91 (d, 1H, *J* = 8.0 Hz), 6.62 (1H, d, *J* = 8.0 Hz, H_p). ^{13}C NMR (δ, ppm, DMSO-d_6): 196.9 (CO), 194.2 (CO), 162.3 (CN_4), 157.3, 154.3, 146.5, 139.7, 130.3, 129.6, 127.7, 126.7, 116.3, 115.5, 112.3. Elemental Analysis: Calc for $C_{22}H_{13}N_6O_4Re$: C (43.21%), H (2.14%), N (13.74%); found C (42.91%), H (1.71%), N (13.54%). Single crystals suitable for X-ray diffraction were grown by slow diffusion of diethyl ether into a dichloromethane solution of the complex.

Synthesis of complexes Re4OMe and Re3OMe

The starting precursor *fac*-[Re(phen)(CO)$_3$Cl] and 1.4 equivalents of the corresponding ligand were combined with 1.4 equivalents of triethylamine in a 3:1 mixture of ethanol and water, and heated at reflux overnight.

Re4OMe. The mixture was cooled to room temperature and then concentrated under reduced pressure. This was cooled in an ice bath and the suspended solids filtered under vacuum to afford a bright yellow solid. Yield: 105 mg (80%). ν_{max} (ATR-FTIR)/cm^{-1}: 3065 w, 2940 w, 2840 w, 2507 w, 2016 s (CO), 1916 s (CO), 1886 s (CO). ^{1}H NMR (δ, ppm, DMSO-d_6): 9.57-9.53 (2H, m), 8.99 (2H, d, *J* = 8.4 Hz), 8.31 (2H, s), 8.13 (2H, d, *J* = 8.3 Hz), 7.42 (2H, d, *J* = 8.8 Hz), 6.84 (2H, d, *J* = 8.8 Hz), 3.69 (3H, s). ^{13}C NMR (δ, ppm, DMSO-d_6): 197.0 (CO), 194.7 (CO), 162.1 (CN_4), 159.5, 154.3, 146.6, 139.8, 130.3, 127.7, 126.7, 121.8, 114.1, 55.1. Elemental Analysis: Calc for $C_{23}H_{15}N_6O_4Re$: C (44.16%), H (2.42%), N (13.43%); found C (44.23%), H (2.56%), N (13.45%). Single crystals suitable for X-ray diffraction were grown by slow diffusion of diethyl ether into a dichloromethane solution of the complex.

Re3OMe. The mixture was cooled in an ice bath and the suspended solids filtered under vacuum to afford a bright yellow solid. This crude solid was purified *via* flash chromatography (Brockmann II neutral alumina) and eluted with dichloromethane until the first fraction was completed, corresponding to the rhenium precursor, then switched to a 1:1 mixture of ethyl acetate and dichloromethane to elute the target compound obtained as a yellow solid after evaporation of the solvents. Yield: 96 mg (73%). ν_{max} (ATR-FTIR)/cm^{-1}: 2021 s (CO), 1930 s (CO), 1877 s (CO). ^{1}H NMR (δ, ppm, DMSO-d_6): 9.56 (2H, d, *J* = 6.8 Hz), 8.99 (2H, d, *J* = 8.4 Hz), 8.31 (2H, s), 8.13 (2H, d, *J* = 8.4 Hz), 7.17 (1H, app. t, *splitting* = 7.9 Hz), 7.08 (1H, d, *J* = 8.8 Hz), 6.90 (1H, s), 6.79 (1H, d, *J* = 7.2 Hz), 3.65 (3H, s). ^{13}C NMR (δ, ppm, DMSO-d_6): 197.0 (CO), 194.2 (CO), 162.0 (CN_4), 159.3, 154.3, 146.6, 139.8, 130.5, 129.9, 127.8, 126.8, 117.9, 114.3, 110.5, 54.9. Elemental Analysis: Calc for $C_{23}H_{15}N_6O_4Re{\cdot}0.6CH_2Cl_2$: C (41.90%), H (2.41%), N (12.42%); found C (41.75%), H (2.37%), N (12.11%). Single crystals suitable for X-ray diffraction were grown by slow diffusion of petroleum spirits into a dichloromethane solution of the complex.

Photophysical measurements

Absorption spectra were recorded at room temperature on a Cary 400 UV VIS spectrophotometer. Uncorrected steady-state emission and excitation spectra were recorded on an Edinburgh FLSP920 spectrometer equipped with a 450 W xenon arc lamp, double excitation and single emission monochromators, and a Peltier-cooled Hamamatsu R928P photomultiplier tube (185–850 nm). Emission and excitation spectra were corrected for source intensity (lamp and grating) and emission spectral response (detector and grating) by a calibration curve supplied with the instrument. According to the approach described by

Demas and Crosby,[47, 48] luminescence quantum yields (Φ_{em}) were measured in optically dilute solutions (OD < 0.1 at excitation wavelength) obtained from absorption spectra on a wavelength scale [nm] and compared to the reference emitter by the following equation:

$$\Phi_x = \Phi_r \left[\frac{A_r(\lambda_r)}{A_x(\lambda_x)}\right]\left[\frac{I_r(\lambda_r)}{I_x(\lambda_x)}\right]\left[\frac{(n_r)^2}{(n_x)^2}\right]\left[\frac{D_x}{D_r}\right]$$

where *A* is the absorbance at the excitation wavelength (λ), *I* is the intensity of the excitation light at the excitation wavelength (λ), *n* is the refractive index of the solvent, D is the integrated intensity of the luminescence and Φ is the quantum yield. The subscripts refer to the reference (*r*) and the sample (*x*), respectively. The quantum yields of the complexes were measured against an air-equilibrated solution of quinine sulfate in 0.1 M H_2SO_4 (Φ = 0.58) used as reference.[49] Emission lifetimes (τ) were determined with the single photon counting technique (TCSPC) with the same Edinburgh FLSP920 spectrometer using a pulsed picosecond LED (EPLED 375, fhwm <800 ps) as the excitation source and the above-mentioned R928P PMT as detector. The goodness of fit was assessed by minimising the reduced χ^2 function and by visual inspection of the weighted residuals. For the photophysical measurements at 77 K, the solutions were placed in quartz tubes (2 mm diameter) and inserted in a special quartz dewar filled with liquid nitrogen. The solvents (dichloromethane and acetonitrile) used in the preparation of the solutions for the photophysical investigations were of analytical spectrometric grade. Degassed solutions were prepared by the freeze–pump–thaw technique (three cycles). Experimental uncertainties are estimated to be ±8% for lifetime determinations, ±15% for quantum yields, and ±2 and ±5 nm for absorption and emission peaks, respectively.

Raman spectroscopy

FT-Raman spectra were measured on solid samples in KBr disks. Spectra were taken using a Bruker Optics MultiRAM spectrometer with liquid nitrogen cooled D418T Germanium detector. 1064 nm excitation was provided by a Nd:YAG laser at 250 mW. Spectra were collected with a resolution of 4 cm^{-1}. Resonance Raman spectra were collected using a previously described set up.[50] Samples were measured in methanol with an excitation wavelength of 350.7 nm generated by a krypton-ion laser (Innova I-302, Coherent Inc) at approximately 40 mW. Spectra were solvent subtracted and baseline corrected.

DFT calculations

Density functional theory (DFT) calculations on the complexes were performed using Gaussian 09[51] and Raman spectra generated using GaussSum.[52] The LANL2DZ effective core potential was used for rhenium and the 6-31G(d) basis set was used for the remaining atoms. The B3LYP[53] functional was utilised in all calculations. Four near isoenergetic configurations; where the tetrazole ligand is rotated with respect to the phen moiety, were optimised for each complex (see SI). The configurations were shown to be local minima through generation of only positive frequencies at each optimised geometry. Predicted Raman spectra were calculated in vacuo and scaled by a factor of 0.975. The Raman spectra showed slight variations between the confirmers, therefore an averaged summation of the four confirmations is presented. The structures were further optimised with an acetonitrile solvent field using the SCRF method and the IEFPCM model. Minima were then also obtained at each rotational configuration. TDDFT calculations were performed on the solvent optimised structures. The transition energies, oscillator strengths and predicted UV-vis spectra were averaged across the configurations to give a predicted spectrum. A Mulliken analysis was performed in order to more clearly illustrate the changes in electron density over different parts of the molecule. Only transitions with $f > 0.01$ are tabulated.

X-ray diffraction analysis

Crystallographic data for the structures were measured at 100(2) K on an Oxford Diffraction Xcalibur or Gemini diffractometer using Mo-Kα radiation (λ= 0.71073 Å). Following LP and absorption corrections, the structures were solved by direct methods and refined against F^2 with full-matrix least-squares using the programs SHELXL-2014 or SHELXL2018.[54] Anisotropic displacement parameters were employed for the non-hydrogen atoms. All hydrogen atoms were added at calculated positions and refined by use of a riding model with isotropic displacement parameters based on those of the parent atom. Crystallographic data for the structures reported in this paper have been deposited at the Cambridge Crystallographic Data Centre. Copies of the data for **Re4OH, Re3OH, Re4OMe and Re3OMe** can be obtained free of charge on application to CCDC, 12 Union Rd, Cambridge CB21EZ, UK (fax +441223336033; email deposit@ccdc.cam.ac.uk).

Crystal data

Re4OH. Formula: $C_{22}H_{13}N_6O_4Re$, M = 611.58. Orthorhombic, space group *Pbca*, a = 13.4719(3), b = 18.1620(5), c = 23.1285(5) Å, V = 5659.0(2) Å^3, Z = 8, D_{calc} = 1.436 Mg m^{-3}, μ = 4.33 mm^{-1}, crystal size = 0.33×0.13×0.09 mm^3. Reflections collected = 35082, unique = 9646, R_{int} = 0.056. Data/restraints/parameters = 9646/0/299, Final R indices ($I > 2\sigma(I)$): R_1 = 0.048, wR_2 = 0.1140 R indices (all data): R_1 = 0.0889, wR_2 = 0.1256. $\Delta\rho_{max, min}$ = 2.56, -1.20 e Å $^{-3}$. CCDC 1917662.

Re3OH. Formula: $C_{22}H_{12}N_6O_4Re$, M = 610.58. Triclinic, space group $P\bar{1}$, a = 9.2949(3), b = 9.5006(3), c = 12.6357(4) Å, α = 95.587(2)°, β = 104.913(3)°, γ = 108.209(3)°, V = 1004.85(6) Å^3, Z = 2, D_{calc} = 2.018 Mg m^{-3}, μ = 6.092 mm^{-1}, crystal size = 0.20×0.145×0.06 mm^3. Reflections collected = 32529, unique = 8860, R_{int} = 0.0575. Data/restraints/parameters = 8860/1/303, GooF = 1.034. Final R indices ($I > 2\sigma(I)$): R_1 = 0.0328, wR_2 = 0.0599. R indices (all data): R_1 = 0.0425, wR_2 = 0.0627. $\Delta\rho_{max, min}$ = 2.114, -1.867 e Å $^{-3}$. CCDC 1917663.

Re4OMe. Formula: $C_{23}H_{15}N_6O_4Re$, M = 625.61. Monoclinic, space group $P2_1/n$, a = 10.0897(10), b = 10.8804(10), c = 19.7094(3) Å, β = 95.7110(10)°, V = 2152.96(4) Å^3, Z = 4, D_{calc} = 1.930 Mg m^{-3}, μ = 5.689 mm^{-1}, crystal size = 0.61×0.32×0.16 mm^3. Reflections collected = 79395, unique = 11957, R_{int} = 0.0328. Data/restraints/parameters = 11957/0/308, GooF =

1.094. Final *R* indices ($I > 2\sigma(I)$): R_1 = 0.0205, wR_2 = 0.0458. *R* indices (all data): R_1 = 0.0238, wR_2 = 0.0469. $\Delta\rho_{max, min}$ = 1.556, -0.633 e Å^{-3}. CCDC 1917664.

Re3OMe. Formula: $C_{23}H_{15}N_6O_4Re$, M = 625.61. Monoclinic, space group $P2_1/n$, a = 9.7182(2), b = 10.7464(2), c = 20.5528(3) Å, β = 99.7700(10)°, V = 2115.31(7) Å^3, Z = 4, D_{calc} = 1.964 Mg m^{-3}, μ = 5.790 mm^{-1}, crystal size = 0.37×0.10×0.03 mm^3. Reflections collected = 39769, unique = 7023, R_{int} = 0.0605. Data/restraints/parameters = 7023/0/308, GooF = 1.047. Final *R* indices ($I > 2\sigma(I)$): R_1 = 0.0330, wR_2 = 0.0668. *R* indices (all data): R_1 = 0.0430, wR_2 = 0.0715. $\Delta\rho_{max, min}$ = 1.884, -1.610 e Å^{-3}. CCDC 1917665.

Determination of lipophilicity

The *n*-octanol/water distribution coefficients (log$D_{7.4}$) of the complexes were measured using the shake-flask method.[45] The absorption profile of the complex in each phase was measured by UV-VIS spectroscopy. The absorbance at 280 nm was recorded and used to determine the log $D_{7.4}$ value using the formula:

$$\text{Log } D_{7.4} = \log A_o - \log A_w$$

Where A_o and A_w are the absorbance values of the complex in the *n*-octanol and water phases measured at λ = 280 nm respectively.

Biological testing

The JU77 human mesothelioma cell line was derived from the pleural effusion of a patient[55] and RAW264.7 murine macrophage cells were a kind gift from Jay Steer (University of Western Australia, Perth, Australia). Both cell types were cultured in RPMI-1640 (Life Technologies, Carlsbad, CA) supplemented with 10% Foetal Bovine Serum (FBS) (HyClone, Thermo Scientific, Waltham, MA), 2 mM L-Glutamine, penicillin-streptomycin (100 units/mL) and 10 mM HEPES buffer (all from Life Technologies). Cells were maintained in a humidifier at 37 °C and 5% CO_2 and subcultured when they were 70-80% confluent. RAW 264.7 cells were used at a passage number <20 for all experiments to ensure maintenance of their macrophage characteristics.

JU77 human mesothelioma cells (5 × 10^4) were incubated with the complexes at concentrations of 5 μM, 10 μM and 20 μM for 30 min at 37°C in CO_2. Cells were then washed with PBS, centrifuged at 1200 rpm for 5 min at RT and the pellet resuspended in 500 μL of PBS plus 0.5 μL Zombie NIR (BioLegend, San Diego, CA) with an Ex_{max} of 719nm and Em_{max} of 746nm. After 30 min, cells were washed with 10%FBS/1%BSA in PBS, centrifuged at 1200 rpm for 5 min at RT, and the pellet resuspended in 100 μL PBS. Samples were read immediately using an LSR Fortessa flow cytometer (BD Biosciences, San Jose, CA) and the data analysed using FlowJo software, version 10.0.8 (TreeStar, Oregon, USA).

RAW 264.7 cells (5 × 10^5) were seeded in a 35mm high μ-Dish (Ibidi GmbH, Martinsried, Germany) were cultured for 2 days, then washed once with serum free RPMI1640 and incubated with 10 μM of the complex for 30 min at RT. Cells were then fixed with 4% paraformaldehyde in PBS and imaged using an UltraVIEW VoX Spinning Disc Confocal Microscope (PerkinElmer, Waltham, MA). Images were analysed using the Volocity software (PerkinElmer).

Statistical analysis

Results were expressed as mean ± standard error of mean (SEM) for the values obtained from three independent experiments. Statistical analysis was performed using one-way analysis of variance (ANOVA). The values $P < 0.05$ were considered significant.

Acknowledgements

The authors would like to thank Curtin for the APA scholarships to NA and BS. MM wishes to thank the ARC for funding (FT130100033 and LE130100052). Support from the MacDiarmid Institute is greatly acknowledged.

Notes and references

1 H. C. Schmidt, C. B. Larsen and O. S. Wenger, *Angew. Chem. Int. Ed.*, 2018, **57**, 6706.
2 A. Pannwitz and O. S. Wenger, *Chem. Commun.*, 2019, **55**, 4004.
3 A. M.-H. Yip and K. K.-W. Lo, *Coord. Chem. Rev.*, 2018, **361**, 138.
4 L. A. Worl, R. Duesing, P. Chen, L. D. Ciana and T. J. Meyer, *Dalton Trans.*, 1991, 849.
5 D. Stufkens, *Coord. Chem. Rev.*, 1998, **177**, 127.
6 L. Sacksteder, M. Lee, J. N. Demas and B. A. Degraff, *J. Am. Chem. Soc.* , 1993, **115**, 8230.
7 Q. Zhao, C. Huang and F. Li, *Chem. Soc. Rev.*, 2011, **40**, 2508.
8 A. J. Amoroso, R. J. Arthur, M. P. Coogan, J. B. Court, V. Fernández-Moreira, A. J. Hayes, D. Lloyd, C. Millet and S. J. A. Pope, *New J. Chem.*, 2008, **32**, 1097.
9 K. K.-W. Lo, M.-W. Louie, K.-S. Sze and J. S.-Y. Lau, *Inorg. Chem.*, 2008, **47**, 602.
10 K. Kam-Wing Lo, D. Chun-Ming Ng, W.-K. Hui and K.-K. Cheung, *J. Chem. Soc. Dalton Trans.*, 2001, 2634.
11 K. Yin Zhang, K. Ka-Shun Tso, M.-W. Louie, H.-W. Liu and K. K.-W. Lo, *Organometallics*, 2013, **32**, 5098.
12 M.-W. Louie, A. W.-T. Choi, H.-W. Liu, B. T.-N. Chan and K. K.-W. Lo, *Organometallics*, 2012, **31**, 5844.
13 A. W.-T. Choi, M.-W. Louie, S. P.-Y. Li, H.-W. Liu, B. T.-N. Chan, T. C.-Y. Lam, A. C.-C. Lin, S.-H. Cheng and K. K.-W. Lo, *Inorg. Chem.*, 2012, **51**, 13289.
14 A. J. Amoroso, M. P. Coogan, J. E. Dunne, V. Fernández-Moreira, J. B. Hess, A. J. Hayes, D. Lloyd, C. Millet, S. J. A. Pope and C. Williams, *Chem. Commun.*, 2007, 3066.
15 V. Fernández-Moreira, F. L. Thorp-Greenwood, A. J. Amoroso, J. Cable, J. B. Court, V. Gray, A. J. Hayes, R. L. Jenkins, B. M. Kariuki, D. Lloyd, C. O. Millet, C. F. Williams and M. P. Coogan, *Org. Biomol. Chem.*, 2010, **8**, 3888.
16 R. G. Balasingham, F. L. Thorp-Greenwood, C. F. Williams, M. P. Coogan and S. J. A. Pope, *Inorg. Chem.*, 2012, **51**, 1419.
17 M. Yu, Q. Zhao, L. Shi, F. Li, Z. Zhou, H. Yang, T. Yi and C. Huang, *Chem. Commun.*, 2008, 2115.

18 Q. Zhao, M. Yu, L. Shi, S. Liu, C. Li, M. Shi, Z. Zhou, C. Huang and F. Li, *Organometallics*, 2010, **29**, 1085.
19 P. R. Ogilby, *Chem. Soc. Rev.*, 2010, **39**, 3181.
20 R. Rodriguez, *Biorg. Med. Chem.*, 2019, **27**, 2281.
21 R. A. Kirgan, B. P. Sullivan and D. P. Rillema, Topics in Current Chemistry, eds. V. Balzani and S. Campagna, Springer Berlin Heidelberg, Berlin, Heidelberg, 2007, **281**, 45.
22 C. A. Bader, R. D. Brooks, Y. S. Ng, A. Sorvina, M. V. Werrett, P. J. Wright, A. G. Anwer, D. A. Brooks, S. Stagni, S. Muzzioli, M. Silberstein, B. W. Skelton, E. M. Goldys, S. E. Plush, T. Shandala and M. Massi, *RSC Adv.*, 2014, **4**, 16345.
23 C. A. Bader, T. Shandala, E. A. Carter, A. Ivask, T. Guinan, S. M. Hickey, M. V. Werrett, P. J. Wright, P. V. Simpson, S. Stagni, N. H. Voelcker, P. A. Lay, M. Massi, S. E. Plush and D. A. Brooks, *PLoSONE*, 2016, **11**, e0161557.
24 A. Sorvina, C. A. Bader, C. Caporale, E. A. Carter, I. R. D. Johnson, E. J. Parkinson-Lawrence, P. V. Simpson, P. J. Wright, S. Stagni, P. A. Lay, M. Massi, D. A. Brooks and S. E. Plush, *Oncotarget*, 2018, **9**, 35541.
25 C. A. Bader, A. Sorvina, P. V. Simpson, P. J. Wright, S. Stagni, S. E. Plush, M. Massi and D. A. Brooks, *FEBS Lett.*, 2016, **590**, 3051.
26 D. Aigner, S. A. Freunberger, M. Wilkening, R. Saf, S. M. Borisov and I. Klimant, *Anal. Chem.*, 2014, **86**, 9293.
27 C. Bronner and O. S. Wenger, *Phys. Chem. Chem. Phys.*, 2014, **16**, 3617.
28 W. Herzog, C. Bronner, S. Löffler, B. He, D. Kratzert, D. Stalke, A. Hauser and O. S. Wenger, *ChemPhysChem*, 2013, **14**, 1168.
29 M. Kuss-Petermann, H. Wolf, D. Stalke and O. S. Wenger, *J. Am. Chem. Soc*, 2012, **134**, 12844.
30 Y. G. Isgor and E. U. Akkaya, *Tetrahedron Lett.*, 1997, **38**, 7417.
31 R. P. Cox, H. F. Higginbotham, B. A. Graystone, S. Sandanayake, S. J. Langford and T. D. M. Bell, *Chem. Phys. Lett.*, 2012, **521**, 59.
32 C. Bronner and O. S. Wenger, *Inorg. Chem.*, 2012, **51**, 8275.
33 D. G. Whitten, *Acc. Chem. Res.*, 1980, **13**, 83.
34 K. Chanawanno, J. T. Engle, K. X. Le, R. S. Herrick and C. J. Ziegler, *Dalton Trans.*, 2013, **42**, 13679.
35 W. Liu and K. Heinze, *Dalton Trans.*, 2010, **39**, 9554.
36 K. Koguro, T. Oga, S. Mitsui and R. Orita, *Synthesis*, 1998, 910.
37 M. V. Werrett, D. Chartrand, J. D. Gale, G. S. Hanan, J. G. MacLellan, M. Massi, S. Muzzioli, P. Raiteri, B. W. Skelton, M. Silberstein and S. Stagni, *Inorg. Chem.*, 2011, **50**, 1229.
38 P. J. Wright, S. Muzzioli, M. V. Werrett, P. Raiteri, B. W. Skelton, D. S. Silvester, S. Stagni and M. Massi, *Organometallics*, 2012, **31**, 7566.
39 L. Flamigni, A. Barbieri, C. Sabatini, B. Ventura and F. Barigelletti, Topics in Current Chemistry, eds. V. Balzani and S. Campagna, Springer Berlin Heidelberg, Berlin, Heidelberg, 2007, **281**, 143.
40 W.-M. Xue, M. C.-W. Chan, Z.-M. Su, K.-K. Cheung, S.-T. Liu and C.-M. Che, *Organometallics*, 1998, **17**, 1622.
41 E. V. Efremov, F. Ariese and C. Gooijer, *Anal. Chim. Acta*, 2008, **606**, 119.
42 R. Horvath and K. C. Gordon, *Coord. Chem. Rev.*, 2010, **254**, 2505.
43 R. J. H. Clark and T. J. Dines, *Angew. Chem. Int. Ed.*, 1986, **25**, 131.
44 M. V. Werrett, P. J. Wright, P. V. Simpson, P. Raiteri, B. W. Skelton, S. Stagni, A. G. Buckley, P. J. Rigby and M. Massi, *Dalton Trans.*, 2015, **44**, 20636.
45 W. Huber, R. Linder, J. Niesel, U. Schatzschneider, B. Spingler and P. C. Kunz, *Eur. J. Inorg. Chem.*, 2012, 3140.
46 J. L. Wedding, H. H. Harris, C. A. Bader, S. E. Plush, R. Mak, M. Massi, D. A. Brooks, B. Lai, S. Vogt, M. V. Werrett, P. V. Simpson, B. W. Skelton and S. Stagni, *Metallomics*, 2017, **9**, 382.
47 G. A. Crosby and J. N. Demas, *J. Am. Chem. Soc.*, 1971, **93**, 2841.
48 G. A. Crosby and J. N. Demas, *J. Phys. Chem.*, 1971, **75**, 991.
49 D. F. Eaton, *Pure Appl. Chem.*, 1988, **60**, 1107.
50 R. Horvath, M. G. Fraser, S. A. Cameron, A. G. Blackman, P. Wagner, D. L. Officer and K. C. Gordon, *Inorg. Chem.*, 2013, **52**, 1304.
51 M. J. T. Frisch, G. W.; Schlegel, H. B.; Scuseria, G. E.; Robb, M. A.; Cheeseman, J. R.; Scalmani, G.; Barone, V.; Mennucci, B.; Petersson, G. A.; Nakatsuji, H.; Caricato, M.; Li, X.; Hratchian, H. P.; Izmaylov, A. F.; Bloino, J.; Zheng, G.; Sonnenberg, J. L.; Hada, M.; Ehara, M.; Toyota, K.; Fukuda, R.; Hasegawa, J.; Ishida, M.; Nakajima, T.; Honda, Y.; Kitao, O.; Nakai, H.; Vreven, T.; Montgomery Jr., J. A.; Peralta, J. E.; Ogliaro, F.; Bearpark, M. J.; Heyd, J.; Brothers, E. N.; Kudin, K. N.; Staroverov, V. N.; Kobayashi, R.; Normand, J.; Raghavachari, K.; Rendell, A. P.; Burant, J. C.; Iyengar, S. S.; Tomasi, J.; Cossi, M.; Rega, N.; Millam, N. J.; Klene, M.; Knox, J. E.; Cross, J. B.; Bakken, V.; Adamo, C.; Jaramillo, J.; Gomperts, R.; Stratmann, R. E.; Yazyev, O.; Austin, A. J.; Cammi, R.; Pomelli, C.; Ochterski, J. W.; Martin, R. L.; Morokuma, K.; Zakrzewski, V. G.; Voth, G. A.; Salvador, P.; Dannenberg, J. J.; Dapprich, S.; Daniels, A. D.; Farkas, Ö.; Foresman, J. B.; Ortiz, J. V.; Cioslowski, J.; Fox, D. J. , Gaussian 09, Gaussian, Inc.: Wallingford, CT, USA, 2009.
52 N. M. O'Boyle, A. L. Tenderholt and K. M. Langner, *J. Comput. Chem.*, 2008, **29**, 839.
53 A. D. Becke, *J. Chem. Phys.*, 1993, **98**, 5648.
54 G. M. Sheldrick, *Acta Cryst. C*, 2015, **71**, 3.
55 L. S. Manning, D. Whitaker, A. R. Murch, M. J. Garlepp, M. R. Davis, A. W. Musk and B. W. S. Robinson, *Int. J. Cancer*, 1991, **47**, 285.